SIAM J. APPL. MATH.
Vol. 85, No. 6, pp. 2591–2610

AN INTEGRO-DIFFERENTIAL MODEL OF CADMIUM YELLOW PHOTODEGRADATION*

MAURIZIO CESERI†, ROBERTO NATALINI‡, AND MARIO PEZZELLA§

Abstract. Many paintings from the 19th century have exhibited signs of fading and discoloration, often linked to cadmium yellow, a pigment widely used by artists during that time. In this work, we develop a mathematical model of the cadmium sulfide photocatalytic reaction responsible for these damages. By employing nonlocal integral operators, we capture the interplay between chemical processes and environmental factors, offering a detailed representation of the degradation mechanisms. Furthermore, we present a second order positivity-preserving numerical method designed to accurately simulate the phenomenon and ensure reliable predictions across different scenarios, along with a comprehensive sensitivity analysis of the model.

Key words. integro-differential models, photochemical reactions, cultural heritage, positivity-preserving numerical methods

MSC codes. 45J05, 45D05, 65R20, 65D32, 74A65, 74F25

DOI. 10.1137/24M1709704

1. Introduction.

Cadmium yellow [1, 20, 21], whose synthesis was originally described by Gay-Lussac in 1818, was extensively employed by artists throughout the 19^{th} and 20^{th} centuries, including Pablo Picasso [15, 23], Joan Miró [28], Edvard Munch [31, 39], Henri Matisse [32, 33, 45], Claude Monet [46], James Ensor [49], and Vincent van Gogh [50]. When exposed to light, this synthetic pigment, primarily composed of cadmium sulfide (CdS), undergoes a photocatalytic reaction that results in color degradation, posing a significant challenge to the long-term preservation of paintings and cultural heritage. The first systematic study of the CdS deterioration mechanism dates back to 2005 with the work [30], which investigated paintings from 1887 to 1923 using X-ray diffraction and scanning electron microscopy. Since then, a range of significant multidisciplinary contributions has emerged in the scientific literature, furthering the knowledge on the topic [24, 25, 26, 40, 43, 44].

From a chemical perspective, CdS reacts with environmental humidity and oxygen to form cadmium sulfate ($CdSO_4$), with light acting as an activator. Specifically, since

*Received by the editors November 12, 2024; accepted for publication (in revised form) August 12, 2025; published electronically November 20, 2025.
https://doi.org/10.1137/24M1709704
Funding: This work was supported by project PE 0000020 CHANGES - CUP B53C22003780006, NRP Mission 4 Component 2 Investment 1.3, funded by the European Union - NextGenerationEU, by the National Group for Mathematical Analysis, Probability and their Applications (GNAMPA), and by the Italian National Group for Scientific Computing (GNCS) of the National Institute for Advanced Mathematics (INdAM). The work of the third author was partially supported by the INdAM under the GNCS project CUP E53C23001670001.

†C.N.R. National Research Council of Italy - Institute for Applied Mathematics "M. Picone", Via dei Taurini, 19 - 00185 Rome, Italy (maurizio.ceseri@cnr.it). Deceased on August 5^{th}, 2024.
‡C.N.R. National Research Council of Italy - Institute for Applied Mathematics "M. Picone," Via dei Taurini, 19 - 00185 Rome, Italy (roberto.natalini@cnr.it). Member of the Italian INdAM Research group GNAMPA.
§C.N.R. National Research Council of Italy - Institute for Applied Mathematics "M. Picone," Via P. Castellino, 111 - 80131 Naples, Italy (mario.pezzella@cnr.it). Member of the Italian INdAM Research group GNCS.

the cadmium sulfide behaves as a semiconductor with a definite band-gap energy [19] $E_{bg} = 2.42$ eV, the reaction is initiated by supra-band-gap light with photon energy

$$E_M = \frac{\mathtt{hc}}{\lambda_M} > E_{bg}$$

and therefore by light within a spectral range corresponding to wavelengths shorter than $\lambda_M = 512.331$ nm (here, $c = 2.99792 \cdot 10^{17}$ nm $\cdot$ s^{-1} denotes the speed of light, and $h = 4.13567 \cdot 10^{-15}$ s $\cdot$ eV is the Planck constant). Moreover, experimental studies indicated that the temperature can increase the rate of chemical reactions and then accelerate the deterioration process [43, 44], which is more pronounced with increased relative humidity. The overall process, described in [40] as follows,

$$CdS + 4h^+_{surf} + 2H_2O + O_2 \longrightarrow CdSO_4 + 4H^+, \tag{1.1}$$

results in a noticeable color change and the formation of a thin ($5 - 8$ μm) layer of cadmium sulfate on the paint surface. The objective of this work is twofold. First, due to the absence of similar approaches in the literature, we develop a novel integro-differential mathematical model that represents the photochemical degradation process of cadmium yellow, with particular emphasis on the nonlocal effects of light exposure. Second, to ensure efficient and realistic simulations of the phenomenon, we design an accurate numerical method that unconditionally preserves the essential properties of the continuous model, namely, the positivity and monotonicity of its solutions. The proposed model provides a macroscopic description of the phenomenon based on the assumption that the involved chemical species are homogeneous and ideally undefected. As such, the formulation does not resolve microscopic crystalline structures or changes in the electronic configuration due to defects, and its role has been thoroughly investigated in [25, 26, 34]. While our continuum-level formulation abstracts from these fine scale details, it remains sufficiently general and flexible to capture the essential macroscopic dynamics of the photochemical reactions, assuming that accurate molar absorption coefficients are available to characterize the photochemical rate. In this regard, the integration of atomic-scale insights, such as those derived from quantum simulations, could greatly enhance the predictive capability of our model, providing a multiscale modeling approach that bridges quantum-level phenomena and macroscale degradation behavior. Here, our aim is to construct a comprehensive mathematical framework that enhances the understanding of the phenomenon and supports the development of effective preservation strategies for cultural heritage.

The manuscript is structured as follows. Section 2 presents the derivation of our model and establishes the foundation for the subsequent analysis. In section 3, we introduce a dynamically consistent numerical method and provide evidence of its quadratic convergence and advantageous performance. Some simulations under various scenarios are discussed in section 4. and a detailed local sensitivity analysis of the model is conducted in section 5. Finally, closing remarks and perspectives for future investigation in section 6 conclude the paper.

2. Mathematical Modeling. We develop an integro-differential mathematical model to describe the chemical degradation of a thin cadmium yellow paint with thickness L, exposed to a humidity level $w(z)$ and illumination $I_0(\lambda)$ that are constant over time. In what follows, $z \in [0, L]$ represents the depth within the paint and $\lambda \in [\lambda_m, \lambda_M]$ is the light wavelength. Let $c(z,t)$ and $g(z,t)$ denote the concentrations,

at time $t \in [0, \mathsf{T}]$, of CdS and $CdSO_4$, respectively. The reaction in (1.1) is modeled by the following fully conservative Production-Destruction System (PDS)

$$\begin{cases} \dfrac{\partial c}{\partial t}(z,t) = -k_1(c(\cdot,t),\, g(\cdot,t))\; c(z,t)\; w(z), \\ \dfrac{\partial g}{\partial t}(z,t) = k_1(c(\cdot,t),\, g(\cdot,t))\; c(z,t)\; w(z), \qquad\qquad (z,t) \in [0,L] \times [0,\mathsf{T}], \end{cases} \tag{2.1}$$

where $c_0(z) = c(z,0)$, $g_0(z) = g(z,0)$ are known initial conditions, and $k_1(\cdot)$ is the concentrations-dependent photodegradation rate, which will be defined in detail later. The conservativity property of the PDS (2.1) (we refer to [2] for further details, or to [29] and references therein) ensures that, regardless of the form of $k_1(\cdot)$, the following linear invariant holds

$$c(z,t) + g(z,t) = c_0(z) + g_0(z), \qquad \forall\ (z,t) \in [0,L] \times [0,\mathsf{T}].$$

Therefore, under the assumption that no cadmium sulfate is present at the onset of the process, i.e., $g_0(z) = 0$ for all $0 \le z \le L$, we get $g(z,t) = c_0(z) - c(z,t)$, and the equation for the $CdSO_4$ can be disregarded.

To accurately model the reaction (1.1), the kinetic rate $k_1(\cdot)$ incorporates several dependencies. According to the Beer-Lambert law [16], the light intensity is defined as follows:

$$I\left(\lambda, \int_0^z c(\zeta,t)\; d\zeta\right) = I_0(\lambda) \exp\left\{-\int_0^z \mu_a(\lambda, c(\zeta,t), g(\zeta,t))\; d\zeta\right\}, \qquad \lambda \in [\lambda_m, \lambda_M],$$

where the system's absorbance μ_a reads

$$\mu_a(\lambda, c(z,t), g(z,t)) = \varepsilon_c(\lambda) c(z,t) + \varepsilon_g(\lambda) g(z,t) = (\varepsilon_c(\lambda) - \varepsilon_g(\lambda)) c(z,t) + \varepsilon_g(\lambda) c_0(z),$$

with $\varepsilon_c(\lambda)$ and $\varepsilon_g(\lambda)$ representing the molar absorptivities of CdS and $CdSO_4$, respectively (their relation to reflectance is discussed in Section 4). Here, following the approach in [12, 18, 48], we describe the overall light penetration effect with the term

$$\int_{\lambda_m}^{\lambda_M} \frac{2\hat{I}\left(\lambda, \int_0^z c(\zeta,t)\; d\zeta\right)}{\hat{I}^2\left(\lambda, \int_0^z c(\zeta,t)\; d\zeta\right) + 1}\; d\lambda,$$

where $\hat{I}(\cdot) = I(\cdot)/I_{ref}$, and I_{ref} is a given reference value. Incorporating the effects of light and of the environmental (absolute) temperature T_K via the Arrhenius law [3] into the photocatalytic rate yields

$$k_1(c(\cdot,t),\, g(\cdot,t)) = A \exp\left\{-\frac{E_a}{RT_K}\right\} \int_{\lambda_m}^{\lambda_M} \frac{2\hat{I}(\lambda, \int_0^z c(\zeta,t)\; d\zeta)}{\hat{I}^2(\lambda, \int_0^z c(\zeta,t)\; d\zeta) + 1}\; d\lambda. \tag{2.2}$$

Given the humidity level $w(z)$, the PDS (2.1) then reads

$$\begin{cases} \dfrac{\partial c}{\partial t}(z,t) = -A \exp\left\{-\dfrac{E_a}{RT_K}\right\} w(z)\; c(z,t) \displaystyle\int_{\lambda_m}^{\lambda_M} \frac{2\hat{I}(\lambda, \int_0^z c(\zeta,t)\; d\zeta)}{\hat{I}^2(\lambda, \int_0^z c(\zeta,t)\; d\zeta) + 1}\; d\lambda, \\ \hat{I}\left(\lambda, \displaystyle\int_0^z c(\zeta,t)\; d\zeta\right) = \dfrac{I_0(\lambda)}{I_{ref}} \exp\left\{-\left((\varepsilon_c(\lambda) - \varepsilon_g(\lambda)) \displaystyle\int_0^z c(\zeta,t)\; d\zeta + \varepsilon_g(\lambda) C_0(z)\right)\right\}, \end{cases} \tag{2.3}$$

where $z \in [0, L]$, $t \in [0, \mathsf{T}]$, $C_0(z) = \int_0^z c_0(\zeta)\, d\zeta$, A is the pre-exponential or frequency factor, E_a is the reaction activation energy, and R is the gas constant. For a detailed characterization of the Arrhenius parameters, we refer the reader to [4, Section 17D.2].

Remark 2.1. Model (2.3) does not incorporate material-specific electronic band structure or crystal defects. This level of abstraction allows for a general formulation applicable to a broad class of photochemical systems, provided that the molar absorption coefficients are available. However, a direct consequence of this approach is that isoelectronic compounds with similar band gaps, phase, and initial concentrations cannot be distinguished within the framework (2.3). Their specific characteristics are instead implicitly reflected in the choice of the functions in (2.2), which must be selected with care to represent the photochemical properties of the materials involved.

Remark 2.2. As experimental observations have not yet detected any processes of spatial diffusion, the system in (2.1) does not explicitly account for variations along the variable $z \in [0, L]$. However, the spatial dependence of the phenomenon is incorporated in model (2.3) through the use of nonlinear, nonlocal integral operators.

2.1. Dimensionless Formulation. In this subsection, we reformulate the mathematical model (2.3) in a nondimensional form. Assuming that the reference values

$$[c^{ref}] = \text{mol/cm}^3, \quad [w^{ref}] = \text{mol/cm}^3, \quad [\varepsilon_c^{ref}] = \text{cm}^2/\text{mol}, \quad [\varepsilon_g^{ref}] = \text{cm}^2/\text{mol},$$

are given, we introduce the dimensionless parameters

$$\nu = \frac{\varepsilon_c^{ref}}{\varepsilon_g^{ref}}, \qquad \mu = L c^{ref} \varepsilon_g^{ref}, \qquad \xi = (\lambda_M - \lambda_m) w^{ref} \mathsf{T} A \exp\left\{-\frac{E_a}{R T_K}\right\}. \tag{2.4}$$

Furthermore, denoted by $\Omega = [0, 1]$, we linearly rescale the variables as follows:

$$z \in [0, L] \mapsto \tilde{z} = \frac{z}{L}, \quad t \in [0, \mathsf{T}] \mapsto \tilde{t} = \frac{t}{\mathsf{T}}, \quad \lambda \in [\lambda_m, \lambda_M] \mapsto \tilde{\lambda} = \frac{\lambda - \lambda_m}{\lambda_M - \lambda_m}, \tag{2.5}$$

and define, for $\tilde{z}$, $\tilde{t}$, and $\tilde{\lambda}$ belonging to Ω, the dimensionless functions

$$\begin{aligned}
&\tilde{c}(\tilde{z}, \tilde{t}) = \frac{c(\tilde{z}L, \tilde{t}\mathsf{T})}{c^{ref}}, \qquad \tilde{c}_0(\tilde{z}) = \frac{c_0(\tilde{z}L)}{c^{ref}}, \qquad \tilde{w}(\tilde{z}) = \frac{w(\tilde{z}L)}{w^{ref}}, \\
&\tilde{I}(\tilde{\lambda}) = \frac{I_0(\lambda_m + \tilde{\lambda}(\lambda_M - \lambda_m))}{I_{ref}}, \qquad \tilde{\varepsilon}_g(\tilde{\lambda}) = \frac{\varepsilon_g(\lambda_m + \tilde{\lambda}(\lambda_M - \lambda_m))}{\varepsilon_g^{ref}}, \\
&\tilde{\varepsilon}_c(\tilde{\lambda}) = \frac{\varepsilon_c(\lambda_m + \tilde{\lambda}(\lambda_M - \lambda_m))}{\varepsilon_c^{ref}}, \qquad \tilde{\varepsilon}_\nu(\tilde{\lambda}) = \nu \tilde{\varepsilon}_c(\tilde{\lambda}) - \tilde{\varepsilon}_g(\tilde{\lambda}).
\end{aligned} \tag{2.6}$$

Thus, (2.5) and (2.6) imply that

$$\frac{\partial c}{\partial t}(z, t) = c^{ref} \frac{1}{\mathsf{T}} \frac{\partial \tilde{c}}{\partial \tilde{t}}(\tilde{z}, \tilde{t}), \qquad \int_{\lambda_m}^{\lambda_M} \frac{2\hat{I}(\lambda, \cdot)}{\hat{I}^2(\lambda, \cdot) + 1}\, d\lambda = (\lambda_M - \lambda_m) \int_0^1 \frac{2\hat{I}(\tilde{\lambda}, \cdot)}{\hat{I}^2(\tilde{\lambda}, \cdot) + 1}\, d\tilde{\lambda},$$

$$\hat{I}\left(\lambda, \int_0^z c(\zeta, t)\, d\zeta\right) = \tilde{I}(\tilde{\lambda}) \exp\left\{-L c^{ref} \varepsilon_g^{ref} \left(\tilde{\varepsilon}_\nu(\tilde{\lambda}) \int_0^{\tilde{z}} \tilde{c}(\zeta, \tilde{t})\, d\zeta + \tilde{\varepsilon}_g(\tilde{\lambda}) \int_0^{\tilde{z}} \tilde{c}_0(\zeta)\, d\zeta\right)\right\}.$$

From now on, the initial CdS concentration is assumed to be constant in space, so that $c_0(z) = c^{ref}$ for all $z \in [0, L]$, and $\tilde{c}_0(\tilde{z}) = 1$ for all $\tilde{z} \in \Omega$. Moreover, we exclusively refer to the nondimensional variables and functions, which, for simplicity, will still be denoted without the tilde.

Model (2.3) is then restated as follows:

$$\frac{\partial c}{\partial t}(z,t) = -\xi\ w(z)c(z,t)\int_0^1 \frac{2\hat{I}\left(\lambda, z, \int_0^z c(\zeta,t)\ d\zeta\right)}{\hat{I}^2\left(\lambda, z, \int_0^z c(\zeta,t)\ d\zeta\right)+1}\ d\lambda, \qquad (z,t)\in\Omega\times\Omega, \tag{2.7}$$

with $\lambda \in \Omega$ and

$$\hat{I}\left(\lambda, z, \int_0^z c(\zeta,t)\ d\zeta\right) = I(\lambda)\exp\left\{-\mu\left(\varepsilon_\nu(\lambda)\int_0^z c(\zeta,t)\ d\zeta + z\varepsilon_g(\lambda)\right)\right\}. \tag{2.8}$$

Compared to the original formulation (2.3), the dimensionless form (2.7)–(2.8) offers several advantages, including a reduction in the number of parameters.

3. Unconditionally Positive and Monotonic Numerical Method. Since the function $c(z,t)$ represents the dimensionless concentration of a chemical reactant undergoing degradation, our focus is on solutions to (2.7) that are positive and monotonically nonincreasing over time. Remarkably, the development of numerical methods that are both of high order and unconditionally preserve the aforementioned properties poses significant challenges. Nonstandard finite difference discretizations have proven effective in constructing positivity-preserving schemes for integro-differential systems (cf. [35, 37] and references therein). However, the linear convergence of the resulting integrators, which may represent a limitation in simulating realistic scenarios, motivates us to adopt a different approach built on a suitable reformulation of the continuous model.

Straightforward manipulations of (2.7) lead to the following implicit Volterra Integral Equation (VIE) (see, for instance, [7, Section 3.4]):

$$c(z,t) = \exp\left\{-\xi\, w(z)\int_0^t\int_0^1 \frac{2\hat{I}\left(\lambda, z, \int_0^z c(\zeta,\tau)\ d\zeta\right)}{\hat{I}^2\left(\lambda, z, \int_0^z c(\zeta,\tau)\ d\zeta\right)+1}\, d\lambda\, d\tau\right\}, \quad (z,t)\in\Omega\times\Omega, \tag{3.1}$$

with a nonlocal nonlinearity depending on the function $\hat{I}(\cdot)$ defined in (2.8). The idea of the exponential reformulation, introduced in [36, 38] for epidemic models based on second kind convolution VIEs, has the advantage of yielding unconditionally positive schemes when the integrals are approximated. However, although the direct discretization of the embedded memory operators in (3.1) with quadrature rules might provide a viable option for designing accurate schemes, it would result in purely implicit methods and computationally demanding algorithms. Moreover, ensuring unconditional monotonicity of the numerical solution could be challenging in such cases. Here, we introduce a fully explicit, second order scheme which preserves both the positivity and the monotonicity of the solution with no limitations on the discretization steplengths.

Let $\Delta z, \Delta t, \Delta\lambda > 0$ represent the dimensionless spatial, temporal, and frequency stepsizes, respectively. Define N_z, N_t, and N_λ as positive integers such that $1 = N_z\Delta z = N_t\Delta t = N_\lambda\Delta\lambda$. Consider the uniform meshes $z_j = j\Delta z$ for $0 \le j \le N_z$, $t_n = n\Delta t$ for $0 \le n \le N_t$, and $\lambda_l = l\Delta\lambda$ for $0 \le l \le N_\lambda$. We denote by F the function $x \in \mathbb{R}_0^+ \to (2x)/(x^2+1) \in \mathbb{R}_0^+$ and by $c_n^j \approx c(z_j, t_n)$ the approximation of the solution

to (3.1). In this setting, given $c_0^j = 1$, $j = 0, \dots, N_z$, we propose the fully-explicit numerical method

$$\alpha_n^{j,l} = I(\lambda_l) \exp\left\{ -\mu \Delta z \left(\varepsilon_\nu(\lambda_l) \sum_{r=0}^{j-1} c_n^r + j \varepsilon_g(\lambda_l) \right) \right\}, \tag{3.2a}$$

$$p_{n+1}^j = c_n^j \exp\left\{ -\Delta t \Delta\lambda \; \xi w(z_j) \sum_{l=0}^{N_\lambda - 1} F(\alpha_n^{j,l}) \right\}, \tag{3.2b}$$

$$\beta_n^{j,l} = I(\lambda_l) \exp\left\{ -\mu \frac{\Delta z}{2} \left(\varepsilon_\nu(\lambda_l) \left(c_n^0 + 2 \sum_{r=1}^{j-1} c_n^r + c_n^j \right) + 2 j \varepsilon_g(\lambda_l) \right) \right\}, \tag{3.2c}$$

$$\beta_{n+1}^{j,l} = I(\lambda_l) \exp\left\{ -\mu \frac{\Delta z}{2} \left(\varepsilon_\nu(\lambda_l) \left(p_{n+1}^0 + 2 \sum_{r=1}^{j-1} p_{n+1}^r + p_{n+1}^j \right) + 2 j \varepsilon_g(\lambda_l) \right) \right\}, \tag{3.2d}$$

$$\gamma_{n+1}^j = F(\beta_n^{j,0}) + F(\beta_{n+1}^{j,0}) + 2 \sum_{l=1}^{N_\lambda - 1} \left(F(\beta_n^{j,l}) + F(\beta_{n+1}^{j,l}) \right) + F(\beta_n^{j,N_\lambda}) + F(\beta_{n+1}^{j,N_\lambda}), \tag{3.2e}$$

$$c_{n+1}^j = c_n^j \exp\left\{ -\frac{\Delta t}{2} \frac{\Delta\lambda}{2} \; \xi w(z_j) \gamma_{n+1}^j \right\}, \qquad \begin{array}{l} n = 0, \dots, N_t - 1, \\ j = 0, \dots, N_z, \end{array} \tag{3.2f}$$

formulated utilizing a Predictor-Corrector (PC) strategy (see, for instance, [22]). More specifically, a rectangular rule discretization of the integrals in (3.1) is here adopted for the predictive step, while the correction process is designed mimicking the trapezoidal rule (we refer to [17] and references therein for further details on quadrature discretizations).

The following result addresses the unconditional positivity and monotonicity of the PC numerical solution.

THEOREM 3.1. *Consider the system of equations* (3.2) *and assume that* $I(\lambda) \geq 0$ *for all* $\lambda \in \Omega$. *Then, independently of the positive values* Δx, Δt, $\Delta\lambda$, *the solution* $\{c_n^j\}_{n \in \mathbb{N}_0}$, $j \geq 0$ *is positive and nonincreasing with respect to* n.

Proof. The positivity of the sequence $\{c_n^j\}_{n \in \mathbb{N}_0}$ naturally follows, independently of $j \geq 0$, from the last equation in (3.2). By definition, $\beta_n^{j,l}$ and $\beta_{n+1}^{j,l}$ are positive as well, so that $F : \mathbb{R}_0^+ \to \mathbb{R}_0^+$ implies $\gamma_{n+1}^j > 0$ for any n and j. Standard inductive arguments then establish the monotonicity property $c_{n+1}^j \leq c_n^j \leq 1$ for all j and $n \in \mathbb{N}_0$. ∎

3.1. Convergence and Performance. The following result establishes the quadratic convergence of the numerical method (3.2) as $\Delta t, \Delta z, \Delta\lambda \to 0^+$. The proof, which is based on a combination of the arguments presented in [22, Section 3] and [38, Section 3.1], is highly technical and is therefore omitted here because it goes beyond the scope of this work.

THEOREM 3.2. *Assume that the known functions in* (2.7) *are twice continuously differentiable on* Ω. *Denote by* $c(z,t)$, *for* $(z,t) \in \Omega \times \Omega$, *the continuous solution to* (2.7) *and by* $\{c_n^j,\ 0 \leq n \leq N_t,\ 0 \leq j \leq N_z\}$ *its approximation computed by the PC scheme* (3.2). *Let* N_z, N_t, *and* N_λ *be positive integers such that* $1 = N_z \Delta z = N_t \Delta t = N_\lambda \Delta\lambda$. *Then, the global discretization error* $E(\Delta z, \Delta t, \Delta\lambda; t_n, z_j) = |c(z_j, t_n) - c_n^j|$ *satisfies*

$$\max_{\substack{0 \leq j \leq N_z \\ 0 \leq n \leq N_t}} E(\Delta z, \Delta t, \Delta\lambda; t_n, z_j) \leq \Theta(\Delta z^2 + \Delta t^2 + \Delta\lambda^2),$$

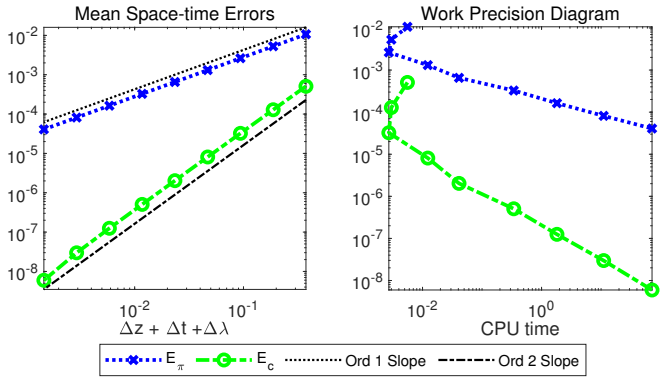

FIG. 1. *Experimental convergence and performance of the P and PC methods.*

with Θ *positive constant independent of the stepsizes. Therefore, the scheme* (3.2) *is convergent of order two.*

Proof. The predictor and corrector schemes used in (3.2) based on the rectangular and trapezoidal quadrature rules, respectively, are specific cases of the Direct Quadrature (DQ) methods introduced in [42]. According to [42, Lemma 4.3, Theorem 4.4], the predictor is linearly convergent, while the corrector achieves quadratic convergence. Hence, the second-order accuracy of the predictor-corrector (PC) integrator (3.2) follows from a straightforward extension of [22, Theorem 2]. ∎

The theoretical aspects of Theorem 3.2, as well as alternative approaches for the simulation of model (2.3), are further investigated and clarified in [42].

In order to experimentally show the convergence property stated with Theorem 3.2, we address equations (2.7)–(2.8) with

$$\begin{array}{ll}\xi=1, & w(z)=1-z,\\ \mu=1, & I(\lambda)=\exp\{\lambda\}-1,\end{array}\quad \varepsilon_\nu(\lambda)=\frac{\lambda-0.9}{1.2-\lambda},\quad \varepsilon_g(\lambda)=1-\lambda+2\lambda^2-\frac{4}{5}\lambda^3, \tag{3.3}$$

where the chosen functions and parameters do not possess any specific physical meaning. We integrate problem (3.3) with the PC scheme (3.2) and compute the mean space-time error E_c and the experimental order of convergence ρ_c as follows:

$$E_c(\Delta z,\Delta t;\Delta\lambda)=\Delta z\Delta t\sum_{j=0}^{N_z}\sum_{n=0}^{N_t}\left|c_n^j-C_n^j\right|,\qquad \rho_c=\log_2\left(\frac{E_c(\Delta z,\Delta t;\Delta\lambda)}{E_c(\frac{\Delta z}{2},\frac{\Delta t}{2};\frac{\Delta\lambda}{2})}\right). \tag{3.4}$$

Here, the reference solution C_n^j is computed by the same method with $\Delta z=\Delta t=\Delta\lambda=2^{-12}$. Figure 1 and Table 1 report the simulation outcomes for different values of the stepsizes and confirm the second order convergence of the PC discretization (3.2). Furthermore, in order to assess the efficiency of the correction process, we compare the PC numerical solution with the one obtained by

$$\pi_{n+1}^j=\pi_n^j\exp\left\{-\Delta t\Delta\lambda\xi w(z_j)\sum_{l=0}^{N_\lambda-1}F\left(I(\lambda_l)\exp\left\{-\mu\Delta z\left(\varepsilon_\nu(\lambda_l)\sum_{r=0}^{j-1}\pi_n^r+j\varepsilon_g(\lambda_l)\right)\right\}\right)\right\}, \tag{3.5}$$

which corresponds to the positive and monotone first order scheme used in (3.2) as the Predictor (P). The work precision diagram in Figure 1 shows the mean errors

TABLE 1
Experimental convergence of the P and the PC methods.

Stepsizes	**Mean Space-time Errors**		**Exp. order**	
$\Delta x = \Delta t = \Delta\lambda$	E_π	E_c	ρ_π	ρ_c
2^{-3}	$1.07 \cdot 10^{-2}$	$5.08 \cdot 10^{-4}$	–	–
2^{-4}	$5.28 \cdot 10^{-3}$	$1.29 \cdot 10^{-4}$	1.02	1.98
2^{-5}	$2.27 \cdot 10^{-3}$	$3.24 \cdot 10^{-5}$	1.01	1.99
2^{-6}	$1.31 \cdot 10^{-3}$	$8.11 \cdot 10^{-6}$	1.00	2.00
2^{-7}	$6.54 \cdot 10^{-4}$	$2.03 \cdot 10^{-6}$	1.00	2.00
2^{-8}	$3.27 \cdot 10^{-4}$	$5.06 \cdot 10^{-7}$	1.00	2.00
2^{-9}	$1.63 \cdot 10^{-4}$	$1.25 \cdot 10^{-7}$	1.00	2.02
2^{-10}	$8.16 \cdot 10^{-5}$	$2.98 \cdot 10^{-8}$	1.00	2.07
2^{-11}	$4.08 \cdot 10^{-5}$	$5.95 \cdot 10^{-9}$	1.00	2.32

TABLE 2
Parameters of the BCT simulation.

Params.	**Descriptions**	**Units**	**Values**
L	Depth of painted layer	cm	$7.00 \cdot 10^{-3}$
T	Reference time	s	$2.30 \cdot 10^{6}$
λ_m	Minimum wavelength	nm	$3.80 \cdot 10^{2}$
λ_M	Band-gap wavelength	nm	$5.12 \cdot 10^{2}$
A	Arrhenius pre-exponential factor	$\mathrm{cm}^2\ \mathrm{mol}^{-1}\mathrm{s}^{-1}$	$1.00 \cdot 10^{8}$
E_a	Activation energy	$\mathrm{J\ mol}^{-1}$	$7.78 \cdot 10^{-19}$
R	Gas constant	$\mathrm{J\ K}^{-1}\ \mathrm{mol}^{-1}$	$8.31 \cdot 10^{0}$
T_K	Temperature	K	$2.98 \cdot 10^{2}$
c^{ref}	Reference CdS concentration	$\mathrm{mol\ cm}^{-3}$	$3.34 \cdot 10^{-2}$
w^{ref}	Humidity reference value	$\mathrm{mol\ cm}^{-3}$	$1.22 \cdot 10^{-6}$
w_b	Humidity lower threshold	$\mathrm{mol\ cm}^{-3}$	$5.77 \cdot 10^{-7}$
ε_c^{ref}	CdS molar absorptivity reference value	$\mathrm{cm}^2\ \mathrm{mol}^{-1}$	$1.64 \cdot 10^{5}$
ε_g^{ref}	$CdSO_4$ molar absorptivity reference value	$\mathrm{cm}^2\ \mathrm{mol}^{-1}$	$6.56 \cdot 10^{5}$
I^{ref}	Irradiance reference value	$\mathrm{W}^2\ \mathrm{m}^{-2}\ \mathrm{nm}^{-1}$	$3.48 \cdot 10^{0}$

Dimensionless Parameters $\mu = 1.53 \cdot 10^{2}, \quad \nu = 2.50 \cdot 10^{-1}, \quad \xi = 3.70 \cdot 10^{3}.$

with respect to the computational efforts and confirms the superior performance of (3.2) compared to (3.5). Remarkably, the PC method achieves an accuracy at least two orders of magnitude higher within a fixed execution time.

4. Numerical Simulations. In this section, we present several experiments in varying scenarios to provide insights into the qualitative behavior of the developed mathematical model. The dimensionless formulation (2.7) is here simulated via the PC method (3.2), choosing the stepsizes $\Delta z = \Delta t = \Delta\lambda = 5 \cdot 10^{-4}$. The dimensional numerical solution is then obtained by reversing the transformations in (2.5).

Test 1: the BCT - For our first experiment, hereafter referred to as the *Base Case Test* (BCT), we assume that the light hits the paint surface at $z = 0$ and set the parameters as detailed in Table 2.

The function $I(\lambda)$, shown in Figure 2 is derived by a local quadratic regression of the emission data for the UV-filtered xenon lamp reported in [41, Fig. 1]. The molar absorptivity $\varepsilon_c(\lambda)$ of cadmium sulfide is obtained from the hex-CdS diffuse reflectance UV-Vis spectra in [40, Supporting Information, Sec. 2.1]. Specifically, given the reflectance $R(\lambda)$ at a relative humidity level of 95%, we assume a zero transmittance and, following the arguments in [27], we compute

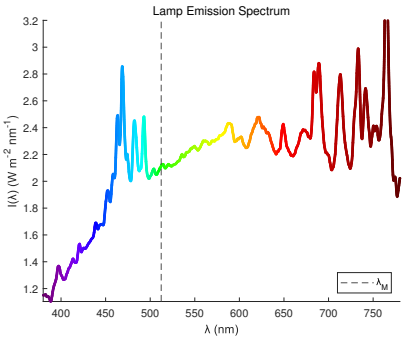

FIG. 2. *Absolute irradiance as a function of the wavelength for the UV-filtered xenon lamp.*

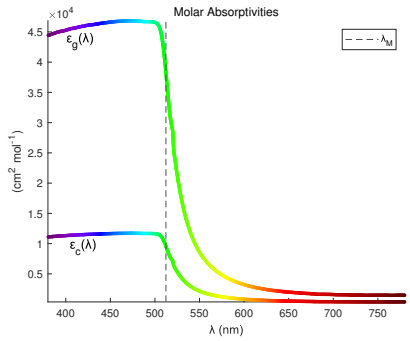

FIG. 3. *Molar absorptivities as functions of the wavelength for the BCT* ($\varepsilon_g(\lambda) = 4\varepsilon_c(\lambda)$).

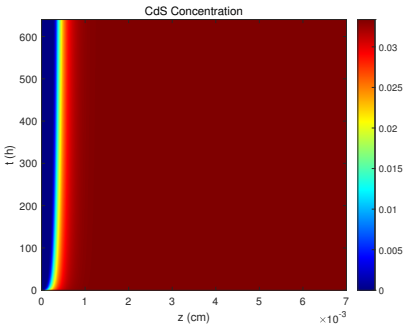

FIG. 4. *BCT: Space-time evolution of the cadmium sulfide concentration.*

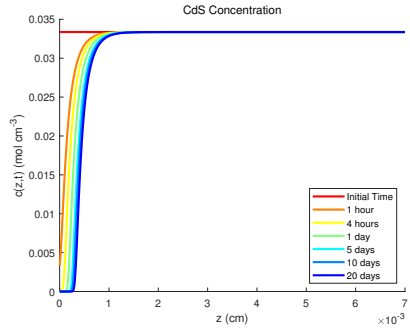

FIG. 5. *BCT: Space evolution of the cadmium sulfide concentration at different times.*

$$\varepsilon_c(\lambda) = -\frac{\log(R(\lambda))}{c^{ref} \cdot L_c} \frac{1}{\varepsilon_c^{ref}}, \qquad \lambda \in \Omega, \tag{4.1}$$

where $L_c = 10^{-4}$ cm represents the thickness of the cadmium sulfate top crust. As for the $CdSO_4$, in absence of experimental data, we assume a proportionality between the two molar absorptivities and take $\varepsilon_g(\lambda) = \nu^{-1}\varepsilon_c(\lambda)$, with ν defined in (2.4) (cf. Figure 3 for the plot of the BCT). Moreover, the infiltration of water is here characterized by the following depth-dependent profile

$$w(z) = \left(1 - \frac{w_b}{w^{ref}}\right)(1 - z), \qquad z \in \Omega, \tag{4.2}$$

where w_b denotes the lowest level of humidity below which the reaction does not occur.

The PC numerical simulations of the BCT in Figures 4 and 5 demonstrate that the photochemical degradation over time predominantly affects the surface, leading to significant variations in the concentrations of CdS and $CdSO_4$ within the shallow regions (cf. Figures 6 and 7). The emergence of an S-shaped pattern in Figures 5 and 7 highlights the formation of cadmium sulfate on the surface and its gradual penetration deeper into the layers. A passivation effect induced by the $CdSO_4$ is evident as well. Indeed, higher concentrations of cadmium sulfate, which is white and highly reflective, visibly retard the overall reaction process.

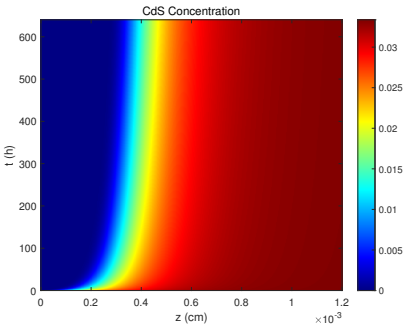

FIG. 6. *BCT: Space-time evolution near the surface of the cadmium sulfide concentration.*

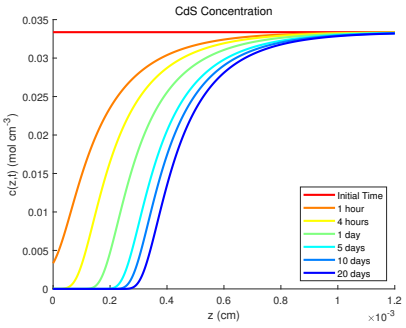

FIG. 7. *BCT: Space evolution near the surface of the cadmium sulfide concentration for different times.*

TABLE 3
Fitted parameters of the separation front logarithmic representation for the BCT simulation.

Threshold Value ψ	**Fitted Parameters** $a(\psi)$	$b(\psi)$	**Mean Fitting Error on** $\{\Sigma_\psi^n\}$
0.9	$6.53 \cdot 10^{-3}$	$9.69 \cdot 10^{-2}$	$9.24 \cdot 10^{-7}$
0.8	$6.57 \cdot 10^{-3}$	$8.09 \cdot 10^{-2}$	$9.21 \cdot 10^{-7}$
0.7	$6.60 \cdot 10^{-3}$	$7.20 \cdot 10^{-2}$	$9.15 \cdot 10^{-7}$

To quantify the passivation effect, given a threshold value $\psi \in \mathring{\Omega}$, we analyze the behavior of the dimensionless separation front

$$\Sigma_\psi(t) = \min\{z \in \Omega \ : \ c(z,t) \geq \psi\}, \qquad t \in \Omega, \tag{4.3}$$

that represents the spatial point from which, at time t, the $CdSO_4$ concentration goes below the threshold $1-\psi$. Figure 8 illustrates the approximated values $\Sigma_\psi^n \approx \Sigma_\psi(t_n)$ derived from the PC numerical solution when $\psi \in \{0.7, 0.8, 0.9\}$. These plots indicate that the separation front progresses linearly respectively to the logarithm of time, whatever the value of ψ. Therefore, we identify $\Sigma_\psi(t)$ in (4.3) with the following function

$$S_\psi(t) = a(\psi) + b(\psi)\log(t),$$

where the threshold-dependent coefficients are determined by a fitting procedure minimizing the mismatch with the Σ_ψ^n values (see Table 3 and Figure 9 for the outcomes). It then follows that $\frac{d^2}{dt^2} S_\psi(t) \propto -\frac{1}{t^2}$ represents an estimate, as time goes by, of the reaction speed reduction due to passivation.

Test 2: the APT - In all simulations, the function $\varepsilon_c(\lambda)$ is derived from data as specified in (4.1). However, due to the lack of experimental data for cadmium sulfate, we assume that $\varepsilon_g(\lambda) = \nu^{-1}\varepsilon_c(\lambda)$. To investigate how this assumption on molar absorptivities affects the degradation kinetics, we perform an *Absorptivity Proportionality Test* (APT).

We explore various choices for the proportionality factor ν reported in Table 4, while maintaining the other parameters consistent with the BCT. Figure 10 reports a comparison of the final CdS concentrations corresponding to the different values of ν. The spatial variation, with respect to the BCT, is reported in Figure 11. Numerical

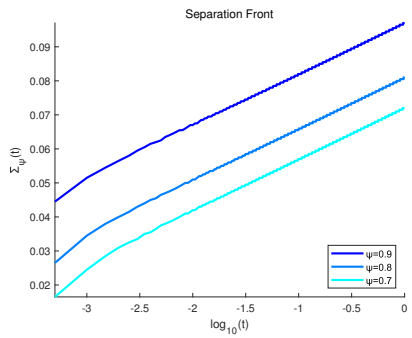

FIG. 8. *BCT: Separation front evolution with respect to the logarithm of time.*

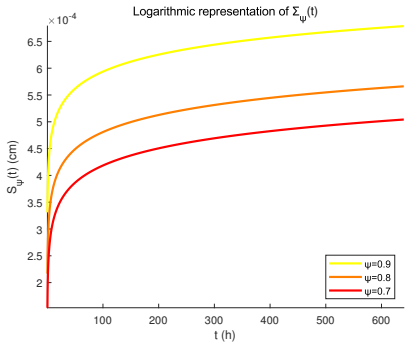

FIG. 9. *BCT: Fitted logarithmic representation of the separation front.*

TABLE 4
Parameters of the APT simulation.

Parameters	**Values**					**Units**
ε_c^{ref}	$1.64 \cdot 10^5$	$1.64 \cdot 10^5$	$1.64 \cdot 10^5$	$1.64 \cdot 10^5$	$1.64 \cdot 10^5$	$cm^2\ mol^{-1}$
ε_g^{ref}	$1.64 \cdot 10^5$	$3.28 \cdot 10^5$	$6.56 \cdot 10^5$	$1.32 \cdot 10^6$	$2.64 \cdot 10^6$	$cm^2\ mol^{-1}$
ν	1	1/2	1/4	1/8	1/16	–

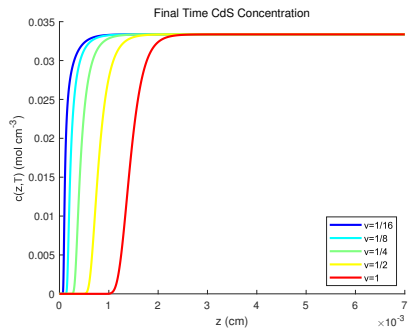

FIG. 10. *APT: Space evolution, after* 20 *days, of the cadmium sulfide concentration for different values of* ν.

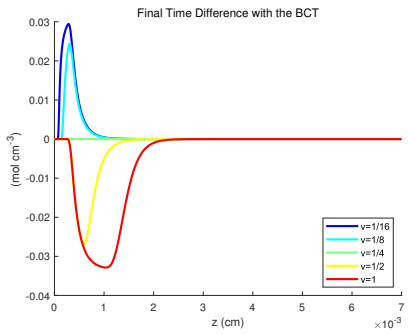

FIG. 11. *APT: Variation in the CdS final concentration with respect to the BCT, i.e., the case of* $\nu = 1/4$.

simulations clearly indicate that as $\varepsilon_g(\lambda)$ increases relatively to $\varepsilon_c(\lambda)$, the degradation effect on CdS decreases. These findings align with expectations because higher molar absorptivity of cadmium sulfate, which tends to accumulate on the surface, leads to greater attenuation of light penetration and its associated effects.

Test 3: the UVT - Until now, we have excluded ultraviolet (UV) radiation from our analysis based on consultations with practitioners who noted that indoor lighting effectively filters out this component. However, given the potential to include paintings exposed outdoors, we conduct a simulation that incorporates these previously omitted wavelengths (for a detailed experimental overview of the effects of UV light on CdS degradation, we refer the reader to [30]). Specifically, for our *Ultraviolet Test* (UVT), we consider $\lambda_m = 200$ nm and employ the functions plotted in Figures 12 and 13, which are derived from the data in [40, 41]. The remaining parameters are equal to those defined in the BCT.

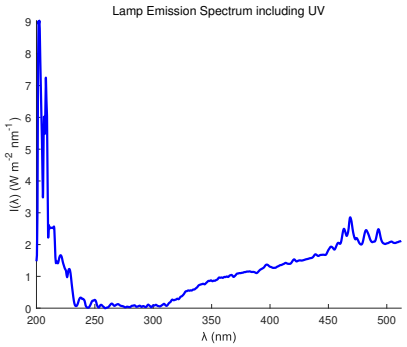

FIG. 12. *UVT: Absolute irradiance as a function of the wavelength for the xenon lamp, including UV radiation.*

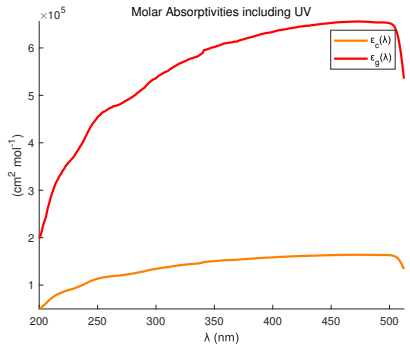

FIG. 13. *UVT: Molar absorptivities as functions of the wavelength, including UV radiation.*

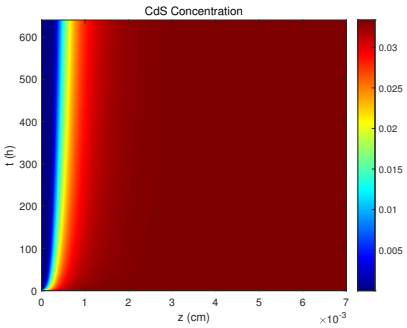

FIG. 14. *UVT: Space-time evolution of the cadmium sulfide concentration.*

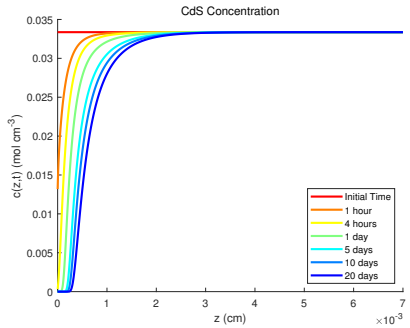

FIG. 15. *UVT: Space evolution of the cadmium sulfide concentration at different times.*

The outcomes of the PC numerical simulations of the UVT are shown in Figures 14 and 15. It is evident that, compared to the BCT, the reaction is slower at the early stages, but then the degradation becomes more pronounced and penetrates deeper into the painting (see also Figures 16 and 17). To quantify this effect, we introduce the cumulative concentration of CdS at time t, defined as follows:

$$C_L^n = \Delta z \sum_{j=0}^{N_z} c_j^n \approx \int_0^L c(\zeta, t_n)\, d\zeta, \qquad n = 0, \dots, N_t, \tag{4.4}$$

whose evolution is represented in Figures 18 and 19. Therefore, considering the impact of UV light, we observe a final increase of 3.5% in the overall deterioration process compared to the base case. These findings are consistent with real-world observations, as increased deterioration is documented in artworks exposed to outdoor environments with natural light.

Test 4: the WPT - We conduct a *Water Penetration Test* (WPT) in order to assess the impact of humidity on the entire process. For the BCT, we assumed the water profile detailed in (4.2), which decreases with increasing depth. Here, given the values of w_b and w^{ref} reported in Table 2, we consider the choices

$$w_s(z) = \chi_{[0,L_s]}(z)\left(1 - \frac{w_b}{w^{ref}}\right)(1 - z) \qquad \text{and} \qquad w_c(z) = \left(1 - \frac{w_b}{w^{ref}}\right),$$

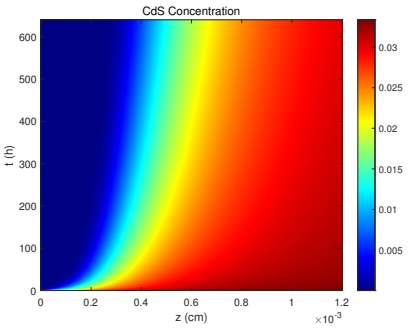

FIG. 16. *UVT: Space-time evolution, near the surface, of the cadmium sulfide concentration.*

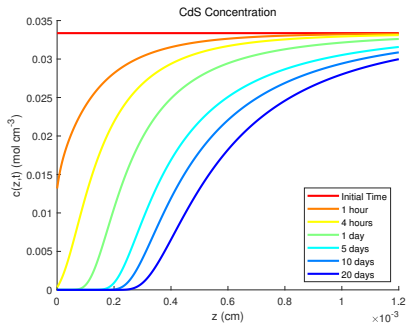

FIG. 17. *UVT: Space evolution, near the surface, of the cadmium sulfide concentration for different times.*

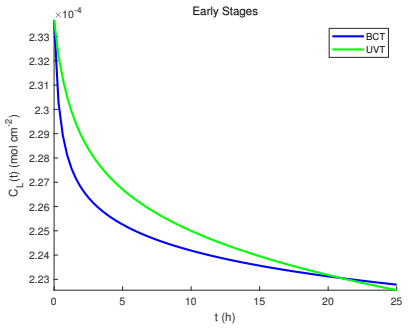

FIG. 18. *UVT: Initial evolution of the cumulative cadmium sulfide concentration.*

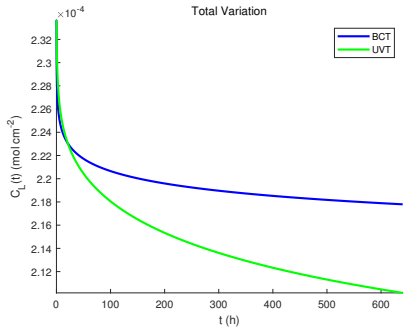

FIG. 19. *UVT: Evolution of the cumulative cadmium sulfide concentration.*

where $\chi_{[0,L_s]}$ represents the indicator function of the interval $[0, L_s]$. From a physical point of view, the function $w_s(z)$ models a heterogeneous medium that is permeable only within a surface sheet of thickness $L_s = 3\mu$m, while it is completely impermeable elsewhere. Conversely, the constant function $w_c(z)$ represents a scenario in which the water content remains uniform throughout the entire painting.

The numerical solution presented in Figure 20 demonstrates that, when $w(z) = w_s(z)$, the reaction is strictly confined to regions where the water penetrates and no degradation occurs for $z > L_s$. Furthermore, the plot in Figure 21, which shows the difference with the numerical solution of the BCT, confirms that for $z \leq L_s$ the reaction behaves exactly the same way as in the base case.

The PC simulations, when $w(z) = w_c(z)$, result in the plots of Figures 22 and 23. In this case, it is evident that the higher water level compared to the BCT enhances the reaction rate, resulting in a lower CdS concentration for the WPT.

Although the current model includes spatially heterogeneous moisture profiles, further developments may consider dynamic water transport influenced by the local chemical composition and degradation state (see, for instance, [14]). Coupling these effects with surface roughness evolution [5, 6] could significantly enhance the predictive capability of the framework.

5. Sensitivity Analysis. Sensitivity analysis (SA) assesses how variations in input parameters impact the model's output and identifies the most influential factors. Conducting the SA on a dimensionless model offers significant advantages, primarily

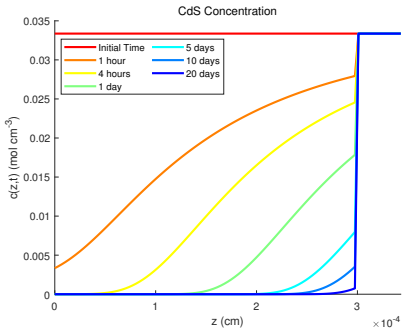

FIG. 20. *WPT: Space evolution, near the superficial sheet, of the cadmium sulfide concentration. Here,* $w(z) = w_s(z)$ *and* $L_s = 3\mu m$.

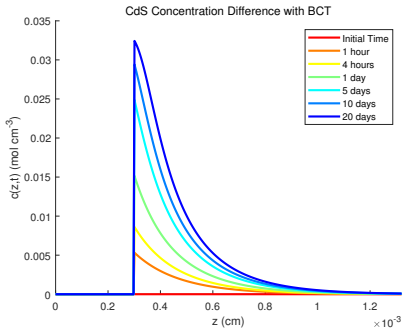

FIG. 21. *WPT: Space evolution, near the surface, of the CdS concentration difference with respect to the BCT. Here,* $w(z) = w_s(z)$ *and* $L_s = 3\mu m$.

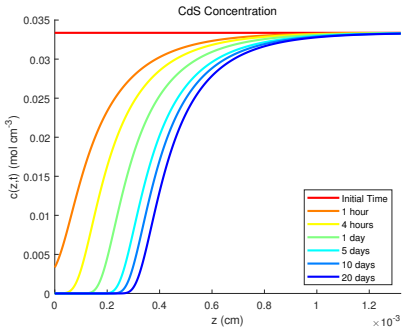

FIG. 22. *WPT: Space evolution, near the surface, of the cadmium sulfide concentration. Here,* $w(z) = w_c(z)$.

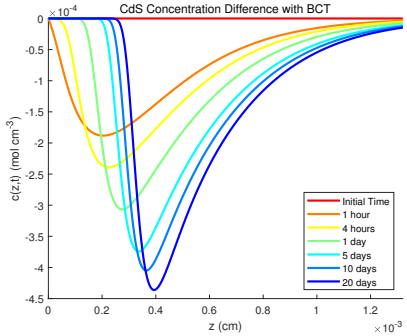

FIG. 23. *WPT: Space evolution, near the surface, of the CdS concentration with respect to the BCT. Here,* $w(z) = w_c(z)$.

due to the reduced number of input variables and the absence of dependencies on measurement units. In this section, we perform a comprehensive local SA of model (2.7). Let ν_0, μ_0, and ξ_0 denote the values of the dimensionless parameters corresponding to the BCT, reported in Table 2. We define the relative overall *CdS* concentration as follows:

$$\mathcal{C}(\nu,\mu,\xi) = \frac{\Delta t \Delta z \sum_{n=0}^{N_t} \sum_{j=0}^{N_z} c_j^n(\nu,\mu,\xi)}{\Delta t \Delta z \sum_{n=0}^{N_t} \sum_{j=0}^{N_z} c_j^n(\nu_0,\mu_0,\xi_0)} \approx \frac{\int_0^1 \int_0^1 c(z,t;\nu,\mu,\xi)\, dz\, dt}{\int_0^1 \int_0^1 c(z,t;\nu_0,\mu_0,\xi_0)\, dz\, dt}, \tag{5.1}$$

where $c_j^n(\nu,\mu,\xi)$ represents the PC numerical solution to (2.7) for the chosen values of the inputs ν, μ, and ξ $(0 \le n \le N_t,\ 0 \le j \le N_z)$.

For our analysis, we consider various values of the input variables (ν,μ,ξ) in a neighborhood of (ν_0,μ_0,ξ_0) and investigate the resulting variations compared to the base case of the overall *CdS* concentration. Specifically, we account for increments and decrements of 1% up to a maximum of 10% for each parameter. For all possible combinations, we apply the numerical method (3.2) with stepsizes $\Delta z = \Delta t = \Delta\lambda = 5 \cdot 10^{-3}$ and compute the corresponding values of the function in (5.1). The described procedure, involving 8000 simulations executed concurrently in a parallel computing

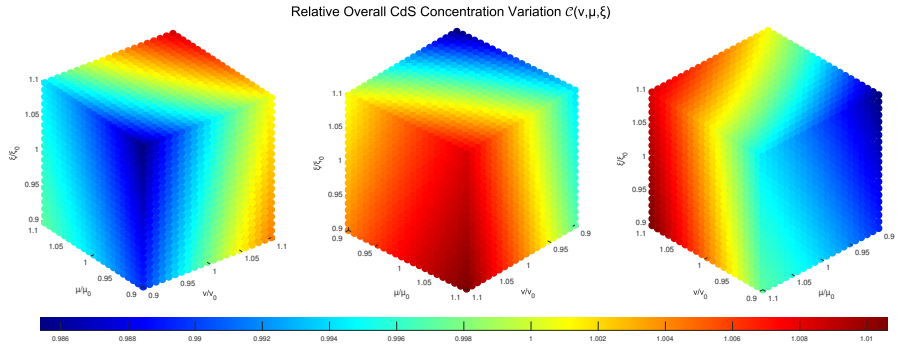

FIG. 24. *Sensitivity analysis of the dimensionless model* (2.7)*: Relative overall CdS concentration as a function of the parameters variation.*

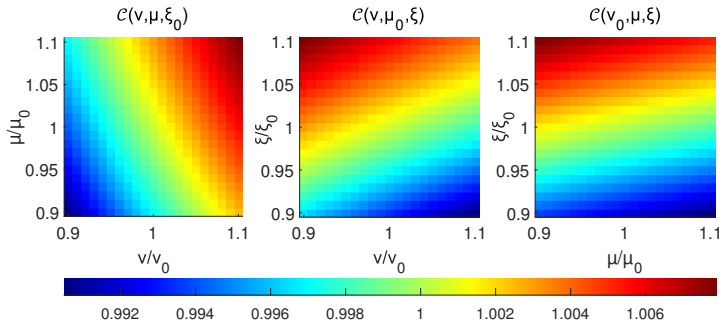

FIG. 25. *Sensitivity analysis of the dimensionless model* (2.7)*: Relative overall CdS concentration as a function of the parameters variation on the planes* $\xi = \xi_0$ *(left panel),* $\mu = \mu_0$ *(central panel), and* $\nu = \nu_0$ *(right panel).*

environment, yields the plots presented in Figures 24 and 25, which illustrate the joint interplay between the input variables.

In order to provide quantitative insights on the sensitivity, we adopt the One-factor-At-a-Time (OAT) SA approach (see, for instance, [47, Section 2.4.2]), which consists of altering only a single input parameter between multiple simulations. The outcomes of the OAT experiments, presented in Table 5, indicate that μ and ξ exert the greatest and the lowest impact on the relative overall CdS concentration, respectively. Following the methodology outlined in [11, 13], we measure the sensitivity via the approximated partial derivatives

$$\frac{\partial \mathcal{C}}{\partial \nu}(\nu_0 \pm \delta_\nu^k, \mu_0, \xi_0) \approx \frac{\mathcal{C}(\nu_0 \pm \delta_\nu^{k+1}, \mu_0, \xi_0) - \mathcal{C}(\nu_0 \pm \delta_\nu^k, \mu_0, \xi_0)}{\delta_\nu^{k+1} - \delta_\nu^k},$$
$$\frac{\partial \mathcal{C}}{\partial \mu}(\nu_0, \mu_0 \pm \delta_\mu^k, \xi_0) \approx \frac{\mathcal{C}(\nu_0, \mu_0 \pm \delta_\mu^{k+1}, \xi_0) - \mathcal{C}(\nu_0, \mu_0 \pm \delta_\mu^k, \xi_0)}{\delta_\mu^{k+1} - \delta_\mu^k},$$
$$\frac{\partial \mathcal{C}}{\partial \xi}(\nu_0, \mu_0, \xi_0 \pm \delta_\xi^k) \approx \frac{\mathcal{C}(\nu_0, \mu_0, \xi_0 \pm \delta_\xi^{k+1}) - \mathcal{C}(\nu_0, \mu_0, \xi_0 \pm \delta_\xi^k)}{\delta_\xi^{k+1} - \delta_\xi^k},$$

where $\delta_\theta^k = \frac{k\theta_0}{100}$ for $\theta \in \{\nu, \mu, \xi\}$ and $k = 0, \ldots, 10$. The numerical simulations in Figure 26 highlight the monotonic behavior of the function $\mathcal{C}$, showing that it increases as ν, or μ increases. Conversely, higher values of the input ξ correspond to lower values of $\mathcal{C}$.

TABLE 5

Sensitivity analysis via the OAT approach of the dimensionless model (2.7)*: For* $\nu = (1 \pm \delta_\nu)\nu_0$, $\mu = (1 \pm \delta_\mu)\mu_0$, *and* $\xi = (1 \pm \delta_\xi)\xi_0$, *the values of* $\mathcal{C}$ *are compared to* $\mathcal{C}(\nu_0, \mu_0, \xi_0) = 1$.

Par. Var. δ_ν	Function $\mathcal{C}$ Variation	Par. Var. δ_μ	Function $\mathcal{C}$ Variation	Par. Var. δ_ξ	Function $\mathcal{C}$ Variation
+10%	+0.321%	+10%	+0.648%	+10%	−0.147%
+9%	+0.292%	+9%	+0.588%	+9%	−0.132%
+8%	+0.264%	+8%	+0.528%	+8%	−0.118%
+7%	+0.234%	+7%	+0.466%	+7%	−0.104%
+6%	+0.203%	+6%	+0.403%	+6%	−0.089%
+5%	+0.172%	+5%	+0.339%	+5%	−0.074%
+4%	+0.139%	+4%	+0.274%	+4%	−0.060%
+3%	+0.106%	+3%	+0.207%	+3%	−0.045%
+2%	+0.072%	+2%	+0.140%	+2%	−0.030%
+1%	+0.036%	+1%	+0.070%	+1%	−0.015%
−1%	−0.038%	−1%	−0.072%	−1%	+0.015%
−2%	−0.076%	−2%	−0.145%	−2%	+0.030%
−3%	−0.116%	−3%	−0.220%	−3%	+0.046%
−4%	−0.157%	−4%	−0.296%	−4%	+0.061%
−5%	−0.199%	−5%	−0.374%	−5%	+0.077%
−6%	−0.243%	−6%	−0.453%	−6%	+0.092%
−7%	−0.288%	−7%	−0.535%	−7%	+0.108%
−8%	−0.334%	−8%	−0.617%	−8%	+0.124%
−9%	−0.382%	−9%	−0.702%	−9%	+0.139%
−10%	−0.431%	−10%	−0.789%	−10%	+0.155%

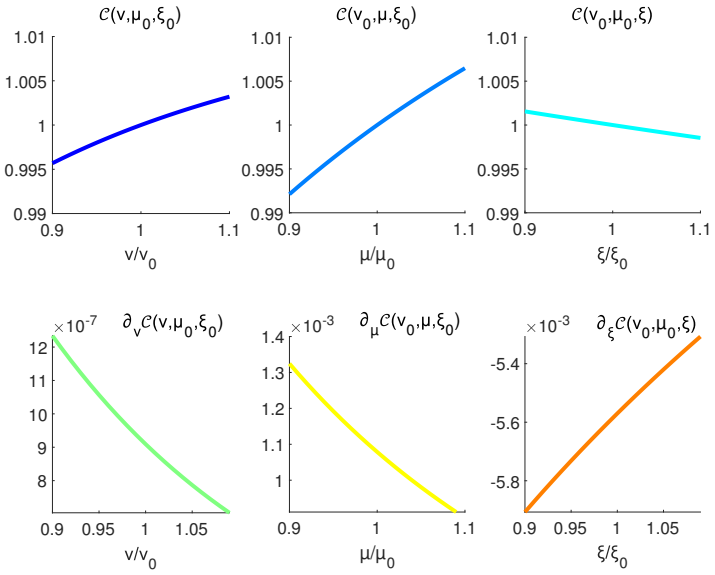

FIG. 26. *Sensitivity analysis via the OAT approach of the dimensionless model* (2.7)*: Relative overall CdS concentrations and corresponding derivatives.*

From our OAT analysis, we conclude that model (2.7) exhibits relatively low sensitivity to perturbations of the parameters. Specifically, small percentage variations in the inputs yield a change in the output (5.1) that is an order of magnitude smaller than the perturbations themselves. This property demonstrates the model's robustness and reliability for practical applications, indicating that minor

inaccuracies in parameter estimation do not significantly affect the representation of the phenomenon.

6. Conclusions and Future Perspectives. In this manuscript, we formulated a comprehensive mathematical framework to describe and simulate the degradation of cadmium yellow in paintings. First, we proposed a model based on nonlinear integro-differential equations that integrates Arrhenius and Beer-Lambert laws to track the photochemical conversion of cadmium sulfide to cadmium sulfate. We then developed a quadratically convergent, positivity-preserving numerical method built on a predictor-corrector discretization of an exponential reformulation of the equations. Furthermore, we provided several simulations which demonstrate the effectiveness of the model in capturing some key aspects of the phenomenon, such as the passivation effect due to $CdSO_4$ accumulation on the surface and the increased degradation resulting from ultraviolet light exposure. These outcomes, along with the sensitivity analysis we performed, confirm the robustness of the proposed framework as a reliable tool for assessing cadmium pigments deterioration.

Given the promising results of our work, there are some potential extensions we plan to investigate in future research. In this context, the implementation of a more involved light-penetration mechanism based on the Kubelka-Munk theory [8, 9, 10] could further enhance the model's accuracy and applicability. A further extension could involve equations capturing the binder's oxidation and yellowing, which may impact the degradation dynamics. Moreover, a calibration of the model's parameters with experimental data could provide valuable insights into the relationship between changes in CdS concentration and observable discoloration in artworks.

The main limitation of the current model is the assumption of a homogeneous and defect-free pigment layer, which excludes microscopic features such as crystalline defects or impurities. As highlighted in recent studies [25, 26], these imperfections may introduce shallow or deep electronic levels that alter the band gap, assumed constant in our framework, as well as the optical and absorption properties. To address this issue, we plan to develop a multiscale extension of the model that incorporates atomistic information into the macroscopic description. A further limitation concerns the static treatment of moisture penetration. In future work, we aim to couple the chemical degradation process with water transport mechanisms that depend on the evolving chemical composition, potentially including changes in surface roughness and texture, following the modeling strategies proposed in [5, 6].

Acknowledgments. Maurizio Ceseri passed away before this manuscript was finalized. We have attempted to present the results of our collaboration in accordance with his high standards. This paper is dedicated to him, whose untimely death is a great loss to us all.

We are grateful to the anonymous reviewers for their insightful comments and constructive suggestions, which enhanced the clarity and depth of the manuscript. We also wish to express our sincere thanks to Letizia Monico, Sara Mattana, Aldo Romani, and Francesca Rosi for their expert advice and valuable discussions on the chemical aspects of this study. The information and insights they provided were essential to the formulation of the model.

This work has been performed under the Project PE 0000020 CHANGES - CUP B53C22003890006, NRP Mission 4 Component 2 Investment 1.3, Funded by the European Union - NextGenerationEU and in the auspices of the *National Group for Mathematical Analysis, Probability and their Applications* (GNAMPA) and of the *Italian National Group for Scientific Computing* (GNCS) of the National Institute

for Advanced Mathematics (INdAM). The work of MP is partially supported by the INdAM under the GNCS Project CUP E53C24001950001.

REFERENCES

[1] Cadmium pigments, Nature, 143 (1939), pp. 891–891, https://doi.org/10.1038/143891a0.
[2] U. an der Heiden and M. C. Mackey, *The dynamics of production and destruction: Analytic insight into complex behavior*, J. Math. Biol., 16 (1982), pp. 75–101, https://doi.org/10.1007/BF00275162.
[3] P. Atkins, J. de Paula, and D. Smith, *Elements of Physical Chemistry*, Oxford University Press, 2016, https://doi.org/10.1093/hesc/9780198727873.001.0001.
[4] P. Atkins, J. d. Paula, and J. Keeler, *Atkins' Physical Chemistry*, Oxford University Press, 2022, https://doi.org/10.1093/hesc/9780198847816.001.0001.
[5] E. Bonetti, C. Cavaterra, F. Freddi, M. Grasselli, and R. Natalini, *A nonlinear model for marble sulphation including surface rugosity: Theoretical and numerical results*, Commun. Pure Appl. Anal., 18 (2019), pp. 977–998, https://doi.org/10.3934/cpaa.2019048.
[6] E. Bonetti, C. Cavaterra, F. Freddi, M. Grasselli, and R. Natalini, *A nonlinear model for marble sulphation including surface rugosity and mechanical damage*, Nonlinear Anal. Real World Appl., 73 (2023), 103886, https://doi.org/10.1016/j.nonrwa.2023.103886.
[7] H. Brunner, *Collocation Methods for Volterra Integral and Related Functional Differential Equations*, Cambridge Monographs on Applied and Computational Mathematics, Cambridge University Press, 2004, https://doi.org/10.1017/CBO9780511543234.
[8] A. Ciani, K.-U. Goss, and R. P. Schwarzenbach, *Determination of molar absorption coefficients of organic compounds adsorbed in porous media*, Chemosphere, 61 (2005), pp. 1410–1418, https://doi.org/10.1016/j.chemosphere.2005.04.082.
[9] A. Ciani, K.-U. Goss, and R. P. Schwarzenbach, *Light penetration in soil and particulate minerals*, Eur. J. Soil Sci., 56 (2005), pp. 561–574, https://doi.org/10.1111/j.1365-2389.2005.00688.x.
[10] A. Ciani, K.-U. Goss, and R. P. Schwarzenbach, *Photodegradation of organic compounds adsorbed in porous mineral layers: Determination of quantum yields*, Environ. Sci. Technol., 39 (2005), pp. 6712–6720, https://doi.org/10.1021/es048096a.
[11] G. Ciavolella, N. Ferrand, M. Sabbah, B. Perthame, and R. Natalini, *A model for membrane degradation using a gelatin invadopodia assay*, Bull. Math. Biol., 86 (2024), pp. 30, https://doi.org/10.1007/s11538-024-01260-w.
[12] F. Clarelli, C. Di Russo, R. Natalini, and M. Ribot, *A fluid dynamics model of the growth of phototrophic biofilms*, J. Math. Biol., 66 (2013), pp. 1387–1408, https://doi.org/10.1007/s00285-012-0538-5.
[13] F. Clarelli, C. Di Russo, R. Natalini, and M. Ribot, *A fluid dynamics multidimensional model of biofilm growth: Stability, influence of environment and sensitivity*, Math. Med. Biol., 33 (2015), pp. 371–395, https://doi.org/10.1093/imammb/dqv024.
[14] F. Clarelli, A. Fasano, and R. Natalini, *Mathematics and monument conservation: Free boundary models of marble sulfation*, SIAM J. Appl. Math., 69 (2008), pp. 149–168, https://doi.org/10.1137/070695125.
[15] D. Comelli, D. MacLennan, M. Ghirardello, A. Phenix, C. Schmidt Patterson, H. Khanjian, M. Gross, G. Valentini, K. Trentelman, and A. Nevin, *Degradation of cadmium yellow paint: New evidence from photoluminescence studies of trap states in Picasso's Femme (Époque des "Demoiselles d'Avignon")*, Anal. Chem., 91 (2019), pp. 3421–3428, https://doi.org/10.1021/acs.analchem.8b04914.
[16] C. D'Aquino, W. Balmant, R. Ribeiro, M. Munaro, J. Vargas, and S. Amico, *A simplified mathematical model to predict PVC photodegradation in photobioreactors*, Polym. Test., 31 (2012), pp. 638–644, https://doi.org/10.1016/j.polymertesting.2012.03.002.
[17] P. Davis, P. Rabinowitz, and W. Rheinbolt, *Methods of Numerical Integration*, Computer Science and Applied Mathematics, Elsevier Science, 2014.
[18] P. Eilers and J. Peeters, *A model for the relationship between light intensity and the rate of photosynthesis in phytoplankton*, Ecol. Model., 42 (1988), pp. 199–215, https://doi.org/10.1016/0304-3800(88)90057-9.
[19] Y. Fan, M. Deng, G. Chen, Q. Zhang, Y. Luo, D. Li, and Q. Meng, *Effect of calcination on the photocatalytic performance of CdS under visible light irradiation*, J. Alloy. Compd., 509 (2011), pp. 1477–1481, https://doi.org/10.1016/j.jallcom.2010.10.044.
[20] E. B. Faulkner and R. J. Schwartz, *High Performance Pigments*, John Wiley & Sons, 2009, https://doi.org/10.1002/9783527626915.

[21] I. Fiedler and M. Bayard, *Cadmium yellows, oranges and reds*, in Artists' Pigments: A Handbook of Their History and Characteristics, Vol. 1, National Gallery of Art. Archetype Publications, 1986, pp. 65–108.

[22] L. Garey, *Predictor-corrector methods for nonlinear Volterra integral equations of the second kind*, BIT, 12 (1972), pp. 325–333, https://doi.org/10.1007/BF01932304.

[23] M. Ghirardello, V. Gonzalez, L. Monico, A. Nevin, D. MacLennan, C. S. Patterson, M. Burghammer, M. Réfrégiers, D. Comelli, and M. Cotte, *Application of synchrotron radiation-based microanalysis on cadmium yellows in Pablo Picasso's Femme*, Microsc. Microanal., 28 (2022), pp. 1504–1513, https://doi.org/10.1017/S1431927622000873.

[24] L. Giacopetti, A. Nevin, D. Comelli, G. Valentini, M. B. Nardelli, and A. Satta, *First principles study of the optical emission of cadmium yellow: Role of cadmium vacancies*, AIP Adv., 8 (2018), 065202, https://doi.org/10.1063/1.5018512.

[25] L. Giacopetti and A. Satta, *Degradation of Cd-yellow paints: Ab initio study of native defects in* 10.0 *surface CdS*, Microchem. J., 126 (2016), pp. 214–219, https://doi.org/10.1016/j.microc.2015.12.005.

[26] L. Giacopetti and A. Satta, *Reactivity of Cd-yellow pigments: Role of surface defects*, Microchem. J., 137 (2018), pp. 502–508, https://doi.org/10.1016/j.microc.2017.12.013.

[27] A. Gobrecht, R. Bendoula, J.-M. Roger, and V. Bellon-Maurel, *Combining linear polarization spectroscopy and the representative layer theory to measure the Beer–Lambert law absorbance of highly scattering materials*, Anal. Chim. Acta, 853 (2015), pp. 486–494, https://doi.org/10.1016/j.aca.2014.10.014.

[28] M. Gomez Lobon, M. Ghirardello, E. Juncosa Darder, C. Palomino Cabello, M. Bauza, M. Cotte, A. Burnstock, A. Nevin, S. R. Amato, F. C. Izzo, and D. Comelli, *A study of cadmium yellow paints from Joan Miró's paintings and studio materials preserved at the Fundació Miró Mallorca*, Heritage Science, 11 (2023), https://doi.org/10.1186/s40494-023-00987-4.

[29] G. Izzo, E. Messina, M. Pezzella, and A. Vecchio, *Modified Patankar Linear Multistep Methods for Production-Destruction Systems*, J. Sci. Comput., 102 (2025), https://doi.org/10.1007/s10915-025-02804-5.

[30] B. Leone, A. Burnstock, C. Jones, P. Hallebeek, K. Keune, and J. Boon *The deterioration of cadmium sulphide yellow artists*, in 14th Triennial Meeting The Hague, 12-16 September 2005 : ICOM Committee for Conservation : preprints volume 2, 2005, pp. 803–813.

[31] B. D. A. Levin, A. C. Finnefrock, A. M. Hull, M. G. Thomas, K. X. Nguyen, M. E. Holtz, U. Plahter, I. Grimstad, J. L. Mass, and D. A. Muller, *Revealing the nanoparticle composition of Edvard Munch's The Scream, and implications for paint alteration in iconic early* 20*th century artworks*, 2019., https://doi.org/10.48550/arXiv.1909.01933.

[32] J. Mass, J. Sedlmair, C. S. Patterson, D. Carson, B. Buckley, and C. Hirschmugl, *SR-FTIR imaging of the altered cadmium sulfide yellow paints in Henri Matisse's Le Bonheur de vivre, – examination of visually distinct degradation regions*, Analyst, 138 (2013), pp. 6032, https://doi.org/10.1039/c3an00892d.

[33] J. L. Mass, R. Opila, B. Buckley, M. Cotte, J. Church, and A. Mehta, *The photodegradation of cadmium yellow paints in Henri Matisse's Le Bonheur de vivre* (1905-1906), Appl. Phys. A, 111 (2012), pp. 59–68, https://doi.org/10.1007/s00339-012-7418-0.

[34] S. Mayda, L. Monico, D. Krishnan, S. De Meyer, M. Cotte, J. Garrevoet, G. Falkenberg, I. C. Sandu, B. Partoens, D. Lamoen, A. Romani, C. Miliani, J. Verbeeck, and K. Janssens, *A combined experimental and computational approach to understanding cds pigment oxidation in a renowned early* 20*th century painting*, Chem. Mater., 35 (2023), pp. 10403–10415, https://doi.org/10.1021/acs.chemmater.3c01470.

[35] E. Messina, M. Pezzella, and A. Vecchio, *A non-standard numerical scheme for an age-of-infection epidemic model*, J. Comput. Dyn., 9 (2022), 239, https://doi.org/10.3934/jcd.2021029.

[36] E. Messina, M. Pezzella, and A. Vecchio, *Positive numerical approximation of integro-differential epidemic model*, Axioms, 11 (2022), pp. 69, https://doi.org/10.3390/axioms11020069.

[37] E. Messina, M. Pezzella, and A. Vecchio, *Nonlocal finite difference discretization of a class of renewal equation models for epidemics*, Math. Biosci. Eng., 20 (2023), pp. 11656–11675, https://doi.org/10.3934/mbe.2023518.

[38] E. Messina, M. Pezzella, and A. Vecchio, *A long-time behavior preserving numerical scheme for age-of-infection epidemic models with heterogeneous mixing*, Appl. Numer. Math., 200 (2024), pp. 344–357, https://doi.org/10.1016/j.apnum.2023.04.009. New Trends in Approximation Methods and Numerical Analysis (FAATNA2022).

[39] L. Monico, L. Cartechini, F. Rosi, A. Chieli, C. Grazia, S. D. Meyer, G. Nuyts, F. Vanmeert, K. Janssens, M. Cotte, W. D. Nolf, G. Falkenberg, I. C. A. Sandu, E. S. Tveit, J. Mass, R. P. de Freitas, A. Romani, and C. Miliani, *Probing the chemistry of CdS paints in The Scream by in situ noninvasive spectroscopies and synchrotron radiation x-ray techniques*, Sci. Adv., 6 (2020), eaay3514, https://doi.org/10.1126/sciadv.aay3514.

[40] L. Monico, A. Chieli, S. De Meyer, M. Cotte, W. de Nolf, G. Falkenberg, K. Janssens, A. Romani, and C. Miliani, *Role of the relative humidity and the Cd/Zn stoichiometry in the photooxidation process of cadmium yellows ($CdS/Cd_{1-x}Zn_xS$) in Oil Paintings*, Chem. A Eur. J., 24 (2018), pp. 11584–11593, https://doi.org/10.1002/chem.201801503.

[41] L. Monico, K. Janssens, M. Cotte, A. Romani, L. Sorace, C. Grazia, B. G. Brunetti, and C. Miliani, *Synchrotron-based X-ray spectromicroscopy and electron paramagnetic resonance spectroscopy to investigate the redox properties of lead chromate pigments under the effect of visible light*, J. Anal. At. Spectrom., 30 (2015), pp. 1500–1510, https://doi.org/10.1039/C5JA00091B.

[42] M. Pezzella, *High order positivity-preserving numerical methods for a non-local photochemical model*, ESAIM, 59 (2025), pp. 1763–1790, https://doi.org/10.1051/m2an/2025041.

[43] F. A. Pisu, C. M. Carbonaro, P. C. Ricci, S. Porcu, and D. Chiriu, *Cadmium yellow pigments in oil paintings: Optical degradation studies utilizing 3D fluorescence mapping supported by Raman spectroscopy and colorimetry*, Heritage, 7 (2024), pp. 2426–2443, https://doi.org/10.3390/heritage7050115.

[44] F. A. Pisu, P. C. Ricci, S. Porcu, C. M. Carbonaro, and D. Chiriu, *Degradation of CdS yellow and orange pigments: A preventive characterization of the process through pump–probe, reflectance X-ray diffraction, and Raman spectroscopy*, Materials, 15 (2022), pp. 5533, https://doi.org/10.3390/ma15165533.

[45] E. Pouyet, M. Cotte, B. Fayard, M. Salomé, F. Meirer, A. Mehta, E. S. Uffelman, A. Hull, F. Vanmeert, J. Kieffer, M. Burghammer, K. Janssens, F. Sette, and J. Mass, *2D X-ray and FTIR micro-analysis of the degradation of cadmium yellow pigment in paintings of Henri Matisse*, Appl. Phys. A, 121 (2015), pp. 967–980, https://doi.org/10.1007/s00339-015-9239-4.

[46] A. Roy, *Monet's Palette in the twentieth century: Water-lilies and irises*, The National Gallery Technical Bulletin, 28 (2007), pp. 58–68, https://www.nationalgallery.org.uk/research/research-resources/technical-bulletin/monet-s-palette-in-the-twentieth-century-water-lilies-and-irises.

[47] A. Saltelli, M. Ratto, T. Andres, F. Campolongo, J. Cariboni, D. Gatelli, M. Saisana, and S. Tarantola, *Global Sensitivity Analysis*, The Primer, Wiley, 2007, https://doi.org/10.1002/9780470725184.

[48] J. Thébault and S. Rabouille, *Comparison between two mathematical formulations of the phytoplankton specific growth rate as a function of light and temperature, in two simulation models (Aster & Yoyo)*, Ecol. Model., 163 (2003), pp. 145–151, https://doi.org/10.1016/S0304-3800(02)00404-0.

[49] G. Van der Snickt, J. Dik, M. Cotte, K. Janssens, J. Jaroszewicz, W. De Nolf, J. Groenewegen, and L. Van der Loeff, *Characterization of a degraded cadmium yellow (CdS) pigment in an oil painting by means of synchrotron radiation based X-ray techniques*, Anal. Chem., 81 (2009), pp. 2600–2610, https://doi.org/10.1021/ac802518z.

[50] G. Van der Snickt, K. Janssens, J. Dik, W. De Nolf, F. Vanmeert, J. Jaroszewicz, M. Cotte, G. Falkenberg, and L. Van der Loeff, *Combined use of synchrotron radiation based micro-X-ray fluorescence, micro-X-ray diffraction, micro-X-ray absorption near-edge, and micro-fourier transform infrared spectroscopies for revealing an alternative degradation pathway of the pigment cadmium yellow in a painting by Van Gogh*, Anal. Chem., 84 (2012), pp. 10221–10228, https://doi.org/10.1021/ac3015627.